Methane adsorption in model mesoporous material

Wei-Shan Chiang and Yun Liu

1. Introduction

Shale gas provided the largest share of U.S. natural gas production in 2013.[1] Its production in U.S. increases from approximately 9.6 billion cubic metre (bcm) in 2001 to 282 bcm in 2015.[2] Recently, it has been shown that the gas storage within the shale rocks is predominately associated with the organic component, the so-called kerogen, in the rocks,[3] which is found to be imbedded within the inorganic matrix and has pores and capillaries of characteristic length scale between 1 nm to 100 nm.[4] For nanometer pores, the pore surface plays important roles both as gas storage location and as flow modulator. The total hydrocarbon reserve is the summation of hydrocarbon adsorbed on the pore surface and the free gas in the pore.[4] In order to better understand the adsorption properties of natural gas, it is crucial to investigate the interaction of the natural gas and the pore surface, and understand the gas adsorption and transportation mechanisms in small pores at the nanometer size length scale.

Ordered mesoporous silica materials have drawn much attention since their discovery in the early 1990s for various applications such as gas storage, heterogeneous catalysis, and separation processes.[5–9] These materials have relatively high surface area and uniform pore size. Their pores can be tailored in a wide range of sizes from about 2 nm up to 30 nm,[10] which cover the essential pore size scale in kerogen and rocks in shale. These properties make the mesoporous silica materials suitable model adsorbents to study the adsorption mechanism of natural gases confined in nanopores. By systematically varying the parameters of pores, it is thus possible to understand the effect of different parameters on the gas adsorption properties.

However, even the gas adsorption in mesoporous model materials is not well understood. For example, in addition to the pore size, the surface properties of small pores is also found to be an important factor in order to reproduce the experimental gas adsorption curves using quench solid density functional theory (QSDFT)[11] and grand canonical Monte Carlo (GCMC)[12] simulation. Hence, there are also fundamental interests to study gas adsorption in this type of materials to understand gas adsorption in pores.

2. Why use SANS to study gas adsorption

Gas adsorption are commonly studied by the isotherm volumetric or gravemetric method. These isotherm measurements report overall the amount of gas adsorption in a sample, from which pore size and porosity information can be obtained. However, these techniques cannot directly probe where the gas molecules are adsorbed in pores. Detailed structure information such as surface roughness, the locations of gas molecules, and the density distribution within the pores are difficult to be probed by either volumetric or gravemetric isotherm measurements.

By properly model the porous materials, small angle neutron scattering (SANS) can be a powerful tool to determine the detailed structure change during the adsorption process. SANS and SAXS

have been demonstrated as a powerful tool to extract the gas adsorption properties in many different type of mateirals.[13–15]

In this study, adsorption behavior of methane onto the surface of a model mesoporous material, MCM-41, is investigated by SANS. Detailed structure determination of gas adsorption and total adsorption amount are achieved by the model fitting. As the first step to understand the gas adsorption properties, we will study the temperature effect on the gas adsorption properties from about 295 K to 20 K.

3. Sample Preparation

A good sample is critical for the success of any experiment.

You will be provided a typical mesoporous silica material, MCM-41. It was synthesized following the methodology reported by Ritter *et al*[16] , and has cylindrical mesopores packed into 2D *p6mm* hexagonal space group.

Deuterated methane, CD_4, will be used as gas adsorbate because its total bound coherent scattering length (= 3.33×10^{-4} Å) is much larger than that of hydrogenated methane, CH_4 (= $- 8.17 \times 10^{-5}$ Å). The scattering length density (SLD) of methane can be calculated by $\rho_{SLD} = \frac{\rho_{mass}}{M_w} N_A b$. ρ_{SLD} and ρ_{mass} are SLD and mass density of methane, respectively. M_w is the molecular weight of methane. At the same amount of mass density change, the SLD change of CD_4 is much larger than that of CH_4. Therefore, the change of SANS intensity is expected to be much larger by using CD_4 instead of CH_4. It should be noted that it is the "contrast of SLD" between different materials that determine the scattering intensity.

To remove the water in MCM-41, the sample will be degassed at 120 ^oC for 1.5 hours before the experiment. The sample will be then loaded in an aluminum sample cell with 1 mm path length. The temperature of the sample can be controlled by a closed cycle refrigerator (CCR). CD_4 will be loaded by a gas loading line linked between the sample cell and a CD_4 gas cart mounted with a pressure sensor. SANS measurement will be first conducted on MCM-41 under vacuum. CD_4 gas will be then loaded *in-situ* to the MCM-41 sample powder. The measurements will be done at different temperatures ranging from 20 K to 295 K. The amount of the MCM-41 sample will be maintained the same during the experiments.

4. Prepare your SANS experiment

4.1. Understand the basics of a SANS instrument

A schematic of the 30-m SANS instrument is shown in Figure 1, and the instrument configuration parameters, and their allowed range for the NG7 SANS, are listed in Table1. In order to determine the instrument configurations we wish to use for gas loading SANS experiments, we will make use of the SASCALC tool available through the NCNR.

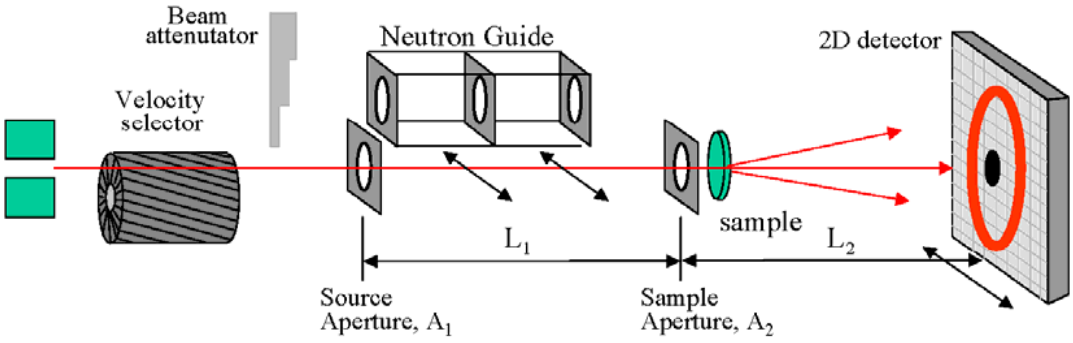

Figure 1. Schematic diagram of the components of the NCNR's 30-m SANS instruments.

Table 1. Instrument configuration parameters and their range of allowed values for the NG7 30-m SANS instrument.

Variable	**Allowed values**
Neutron wavelength	5-20 Å (determined by rotational speed of the velocity selector)
Wavelength spread (FWHM)	0.11, or 0.22 (determined by the spinning frequency and inclination of the velocity selector)
Number of neutron guides	0-8 (determines the beam collimation by changing the distance of the source aperture from the sample)
Source aperture diameter	1.43, 2.22, or 3.81 cm for 0; 5.08 cm for 1-8 guides
Sample-to-detector distance	100-1530 cm
Detector offset	0-25 cm (detector translation perpendicular to beam to extend the *q*-range covered at a given distance)
Sample aperture diameter	0-2.5cm
Beamstop diameter	2.54, 5.08, 7.62, or 10.16 cm
Beam attenuator	10 choices of beam attenuator thickness to reduce beam intensity for sample transmission measurements

4.2. Plan the SANS configurations using SASCALC

For a given set of allowed parameters, SASCALC computes the corresponding *q*-range and the beam intensity (n/sec) on the sample. *q* is the magnitude of scattering vector defined as $q = |\vec{q}| = \frac{4\pi}{\lambda}\sin(\frac{\theta}{2})$, where λ and θ are neutron wave length and scattering angle, respectively. The *q*-range for a particular configuration is determined by the choice of wavelength, detector distance and detector offset. A wavelength of 6 Å is customary for most SANS measurements, as it provides a good compromise between the incident neutron flux and the accessible *q* range, thus minimizing measurement time (longer wavelengths are typically used when very low *q*-values are

desired). Similarly, a wavelength spread of $\Delta\lambda/\lambda$ of 0.11 provides an adequate balance of flux and q -resolution. In general, we choose the largest number of neutron guides (allowed in the desired q -range) in order to maximize the beam intensity on the sample. The source aperture and beam stop diameters will depend on the detector distance chose.

There are several considerations that must be taken into account when determining instrument configurations for SANS measurement. For the short distance, the detector can cover a wide range of q range due to its capability to measure scattered neutrons at large angles, for this distance, we usually put as many neutron guides in as possible. For the long detector distance, we are interested in low-q range, the beam divergence caused by the neutron guides becomes the limiting factors determining its low-q limit. Hence, at the long detector distance, we typically put less neutron guides in. However, the q range covered by short and long distance sometimes may miss some q range. Therefore, it is common to have a configuration at the intermediate distance so that the full q range accessible by the instrument can be covered. The number of configurations needed is determined mainly by the interested q range.

All that remains is to select a combination of sample-to-detector distances and detector offsets that will yield the appropriate q -range for our measurements. For the high-q limit of the instrument, we will use the shortest sample-to detector distance, 100 cm, and the maximum detector offset, 25 cm. We will choose 8 guides at this distance to maximize the neutron flux. The results from SASCALC for these choices are as follows:

Source Aperture Diameter = 5.08 cm
Source to Sample = 387 cm
Sample Aperture to Detector = 105 cm
Beam diameter = 3.14 cm
Beamstop diameter = 2.00 inches
Minimum Q-value = 0.0530 1/Å (sigQ/Q = 14.1 %)
Maximum Horizontal Q-value = 0.6438 1/Å
Maximum Vertical Q-value = 0.3876 1/Å
Maximum Q-value = 0.7174 1/Å (sigQ/Q = 4.8 %)
Beam Intensity = 5214718 counts/s
Figure of Merit = 1.3e+08 Å^2/s
Attenuator transmission = 0.000265 = Atten # 9
Sample Aperture Diameter = 1.27 cm
Number of Guides = 8
Sample Chamber to Detector = 100.0 cm
Sample Position is Chamber
Detector Offset = 25.0 cm
Neutron Wavelength = 5.00 Å
Wavelength Spread, FWHM = 0.115
Sample Aperture to Sample Position = 5.00 cm
Lenses are OUT

For the low-q limit of the instrument, we will use 8.09 Å to take advantage of the focusing lens at NG7 SANS to reach the smallest Q value possible (about 0.001 $Å^{-1}$). The detector has to be at the

longest sample-to detector distance, 1530 cm. The results from SASCALC for these choices are as follows:

Source Aperture Diameter = 1.43 cm
Source to Sample = 1627 cm
Sample Aperture to Detector = 1536 cm
Beam diameter = 1.43 cm
Beamstop diameter = 1.00 inches
Minimum Q-value = 0.0009 1/Å (sigQ/Q = 41.6 %)
Maximum Horizontal Q-value = 0.0162 1/Å
Maximum Vertical Q-value = 0.0162 1/Å
Maximum Q-value = 0.0229 1/Å (sigQ/Q = 5.0 %)
Beam Intensity = 10527 counts/s
Figure of Merit = 6.89e+05 Å^2/s
Attenuator transmission = 0.0527 = Atten # 3
Sample Aperture Diameter = 1.27 cm
Number of Guides = 0
Sample Chamber to Detector = 1531.0 cm
Sample Position is Chamber
Detector Offset = 0.0 cm
Neutron Wavelength = 8.09 Å
Wavelength Spread, FWHM = 0.115
Sample Aperture to Sample Position = 5.00 cm
Lenses are IN

For intermediate q -values, we wish to choose a detector distance such that the q -range will be covered around the peak in the simulated scattering data. After experimenting with a few values of the detector distance in SASCALC, we find that a detector distance of 400 cm with no offset will achieve our objective. We will choose 5 guides, the maximum at this distance, to maximize the count rate on the detector. The results from SASCALC for these choices are as follows:

Source Aperture Diameter = 5.08 cm
Source to Sample = 852 cm
Sample Aperture to Detector = 405 cm
Beam diameter = 4.50 cm
Beamstop diameter = 2.00 inches
Minimum Q-value = 0.0064 1/Å (sigQ/Q = 24.7 %)
Maximum Horizontal Q-value = 0.0620 1/Å
Maximum Vertical Q-value = 0.0620 1/Å
Maximum Q-value = 0.0875 1/Å (sigQ/Q = 5.0 %)
Beam Intensity = 365746 counts/s
Figure of Merit = 2.39e+07 Å^2/s
Attenuator transmission = 0.00643 = Atten # 5
Sample Aperture Diameter = 1.27 cm
Number of Guides = 5
Sample Chamber to Detector = 400.0 cm

Sample Position is		Chamber
Detector Offset =		0.0 cm
Neutron Wavelength =		8.09 Å
Wavelength Spread, FWHM =		0.115
Sample Aperture to Sample Position =	5.00 cm	
Lenses are OUT		

5. Setting up experiments and collecting data on SANS

5.1 Set up the equipment on SANS instrument.

The sample needs to be loaded into a special sample cell, which will be mounted to a bottom loading CCR (closed cycle refrigerator) to control the temperature from about 295 K to 20 K. The left panel of Figure 2 shows the cell mounted on the CCR. There is a gas loading line connecting the cell to a gas loading equipment. During the experiment, there will be an outside cover of the CCR so that we can pull vacuum around the sample cell. The right panel of Figure 2 shows the final setup on a SANS beamline.

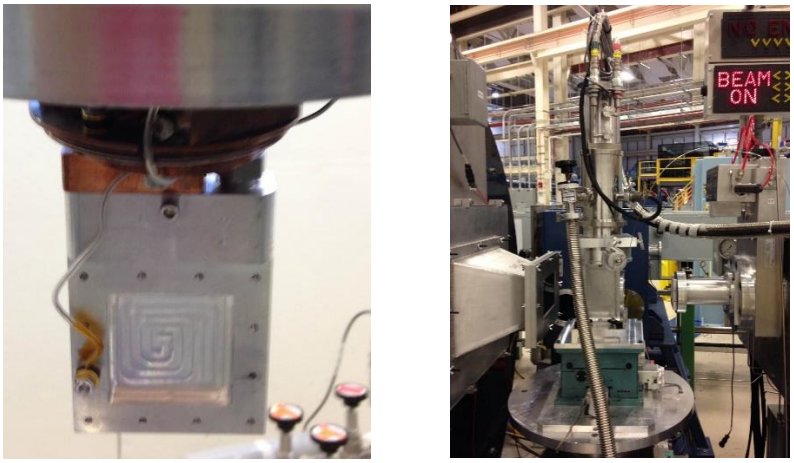

Figure 2. Left panel shows the sample cell mounted on a CCR. Right panel shows the whole setup on a beamline.

Before the experiment, we need to test the sample cell to make sure it will not leak. After the test, the CCR will be ready to be put in the beamline.

5.2 What is needed to be collected in order to have the absolute scattering of your samples.[17]

The absolute intensity is the microscopic scattering cross section of your samples. Ideally, it is a value that only depends on the scattering of your samples, and is independent of SANS instruments used to collect the data. However, the instrument resolution still affects the data. In order to finally obtain the absolute value, certain measurements have to be performed.

In general, scattering intensity (neutron counts) recorded by the detector with the sample in the beam can come from 3 sources: 1) neutrons scattered by the sample itself (the scattering we are interested in); 2) neutrons scattered from something other than the sample, but pass through the sample; and 3) everything else, including neutrons that reach the detector without passing through the sample (stray neutrons or so-called room background) and electronic noise in the detector itself. To separate these three contributions, we need three measurements:

i) Scattering measured with the sample in place (which contains contribution from all 3 sources listed above), denoted $\boldsymbol{I_{sam}}$. This measurement will be made for each sample at different temperatures we are interested in.
ii) Scattering measured with empty cell inside the CCR (which contains contributions from the 2nd and 3rd sources listed above), denoted $\boldsymbol{I_{emp}}$. This measurement will be made at only one temperature (room temperature).
iii) Counts measured with a complete absorber ("blocked beam") at the sample position (which contains only the contribution from the 3rd source listed above), denoted $\boldsymbol{I_{bgd}}$. This measurement will be made only once.

In addition to these three 'scattering' measurements, the transmission (the fraction of the incident beam intensity that passes through the sample without being scattered or absorbed) of the sample and the sample cell must also be measured in order to correctly subtract the contributions to the background and to calibrate the scattering on an absolute cross section scale (see section 6-Data reduction). The transmission is measured by inserting a calibrated attenuator in the incident beam (to reduce the direct beam intensity to an accurately measurable level) and measuring the direct beam intensity with and without the sample in the respective environments. The ratio of these two short measurements (typically 3 minutes each) is the sample (or sample cell) transmission. For gas adsorption SANS measurements, it is important to measure the sample transmission at every temperature because the amount of gas adsorbed changes.

5.3 Counting statistics

A SANS experiment is an example of the type of counting experiments that follow the Poisson distribution. The uncertainty, or more precisely the standard deviation, σ, in the number of counts recorded in time, $I(t)$, is $\sigma \sim \sqrt{I(t)}$. For example, if the accumulated counts are 1000 counts per data point, its standard deviation is $\sqrt{1000} \sim 30$. Hence, a relative uncertainty of about 3 %, which is good enough for most purposes.

A related question is how long should the background and empty cell measurements be counted relative to the sample measurement. The same $\sigma \sim \sqrt{I(t)}$ relationship leads to the following approximate result for the optimal relative counting times

$$\frac{t_{background}}{t_{sample}} \sim \sqrt{\frac{Count\ Rate_{background}}{Count\ Rate_{sample}}}$$

Hence if the scattering from the sample is weak, the background should be counted for as long (but no longer!) as the sample scattering. However, if the sample scattering count rate is, say, 4 times greater than the background rate, the background should be counting only half as long as the sample scattering.

6. Data reduction

6.1 Data reduction procedures[17]

Data reduction begins by correcting the measured scattering from the sample for the sources of background discussed previously, and multiplying the corrected counts by a scaling factor (to remove incidental differences between measurements such as the counting time and sample thickness) that puts the data on an absolute scale of scattering cross section per unit volume. The background-corrected neutron counts, $I_{cor}(q_x,q_y)$, recorded in a detector pixel in a time interval t are related to the differential microscopic scattering cross section (the absolute intensity), $d\Sigma(q_x,q_y)/d\Omega$, through the expression

$$I_{cor}\left(q_x,q_y\right)=\phi\ A\ \Delta\Omega\ \varepsilon\ t\ d\ T\ \frac{d\Sigma\left(q_x,q_y\right)}{d\Omega}$$

where:

ϕ = the neutron flux (neutrons/cm^2-sec) at the sample
A = the area of the beam incident on the sample
d = the sample thickness
T = the transmission of the sample
$\Delta\Omega$ = the solid angle subtended by one pixel of the detector
ε = the detector efficiency, and
t = the counting time.

The incidental instrumental factors can be lumped together into one constant, $K=\phi\ A\ \Delta\Omega\ \varepsilon\ t$, and the intrinsic quantity $d\Sigma(q_x,q_y)/d\Omega$, the differential scattering cross section per unit volume, is obtained by scaling the recorded counts

$$\frac{d\Sigma\left(q_x,q_y\right)}{d\Omega}=\frac{I_{cor}\left(q_x,q_y\right)}{KdT}$$

We now go over the specific steps involved in extracting $d\Sigma(q)/d\Omega$ from the raw data. The raw scattered intensity measured from the sample, I_{sam}, and the empty cell, I_{emp}, can be written as

$$I_{sam}\left(q_x,q_y\right)=KdT_{sample+cell}\left[\left(\frac{d\Sigma\left(q_x,q_y\right)}{d\Omega}\right)_{sam}+\left(\frac{d\Sigma\left(q_x,q_y\right)}{d\Omega}\right)_{emp}\right]+I_{bgd}\left(q_x,q_y\right)$$

$$I_{emp}\left(q_x,q_y\right)=KdT_{cell}\left(\frac{d\Sigma\left(q_x,q_y\right)}{d\Omega}\right)_{emp}+I_{bgd}\left(q_x,q_y\right)$$

where $T_{sample+cell}$ and T_{cell} are the measured transmission of the sample (at each temperature) and the empty cell, respectively. From the above, the background corrected scattering, denoted I_{cor}, is given by

$$I_{cor}\left(q_x, q_y\right) = \left[I_{sam}\left(q_x, q_y\right) - I_{bgd}\left(q_x, q_y\right) \right] - \frac{T_{sample+cell}}{T_{cell}} \left[I_{emp}\left(q_x, q_y\right) - I_{bgd}\left(q_x, q_y\right) \right]$$

Here we assume the neutron flux is stable, and the counting times for sample and sample cell are the same. (In fact, the neutron flux can change with time and depends on reactor stability. This has been considered to monitor the beam flux change in the beamline. The counting times for sample and sample cell can be different too. A scaling factor based on the relative counting time can be applied in the above equation to take this into consideration.) The corrected counts, I_{cor}, are proportional to the quantity of interest, namely the differential scattering cross section. From the above equations,

$$I_{cor}(q_x, q_y) = KdT_{sample+cell}\left(\frac{d\Sigma(q_x, q_y)}{d\Omega} \right)_{sample}$$

The instrumental scale factor, K, will be determined from a measurement of the attenuated direct beam intensity,

$$I_{direct} = KT_{atten}$$

where T_{atten} is the transmission of a calibrated attenuator. The result of the data correction is a two-dimensional absolute, corrected scattering differential scattering cross section $\left(\frac{d\Sigma(q_x, q_y)}{d\Omega} \right)_{sample}$ as a function of the q-values (corresponding to detector pixels) q_x and q_y.

6.2 Examples of reduced data

During our SANS experiment, we will collect the data at different temperatures. Due to the gas adsorption to the samples, the scattering intensity at different temperatures is expected to be different. Figure 3 shows the reduced data collected in a previous experiment. You can see that the scattering intensity is very sensitive to the temperature change.

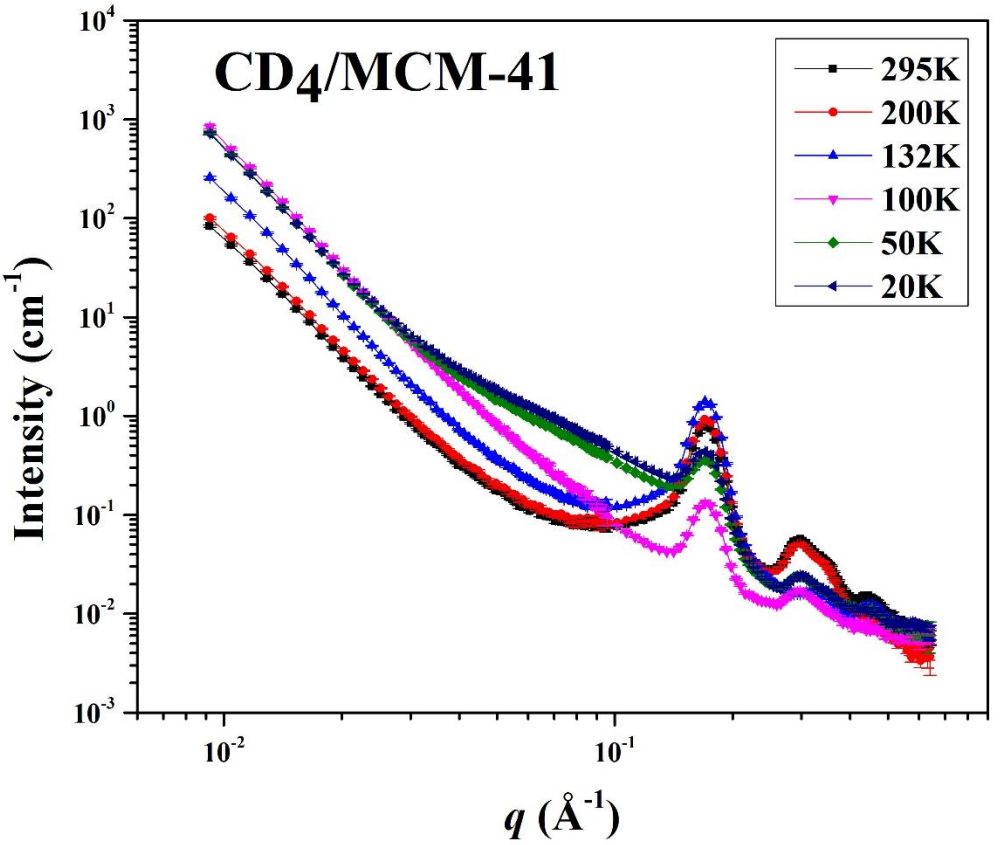

Figure 3. Temperature-dependent SANS data at pressure ≈ 100 kPa for CD_4/MCM-41

The intensity variation with temperature is solely due to the adsorption of CD_4 molecules into the pores because a separate experiment indicates that intensity of empty MCM-41 does not change with temperature in the temperature range being studied.

When temperature decreases from 295 K, the peak intensity first increases gradually and then drops abruptly at certain temperature range, and eventually the intensity increases again.

7. Data analysis

7.1 Scattering models

The small-angle scattering intensity $I(q)$ of powder MCM-41 without gas and MCM-41 loaded with CD_4 can be written as $I(q) = n\langle P(\vec{q})\, S(\vec{q})\rangle$. n is a pre-factor related to the number density of MCM-41 mesopores in the neutron beam. $P(\vec{q})$ is the form factor describing the detailed structure of MCM-41 cylindrical mesopores with or without adsorbed and free CD_4 confined inside. $S(\vec{q})$ is the structure factor characterizing the hexagonally packed cylindrical pores. Because a powder-like sample is used, <…> represents the ensemble average over all possible orientations of the MCM-41 grains. For hexagonally packed cylindrical pores, $S(\vec{q})$ is the summation of the delta

functions located at hexagonal lattice points in reciprocal space, $q_{h,k}$, where *h* and *k* are the Miller indices of the 2D lattice.

For the CD_4 loaded MCM-41 (CD_4/MCM-41) case, cylindrical pores have adsorbed gas molecules on the pore wall and free gas in the pore center. By assuming the interface between the MCM-41 mesopore wall and the adsorbed CD_4 layer is a Gaussian diffuse interface and the interface between the adsorbed layer and the free vapor core is a sharp and smooth interface, $P(\vec{q})$ for CD_4/MCM-41[13] has been shown to be

$$I(q) = C\sum_{h,k}\left\{\begin{array}{l}\frac{1}{q_{h,k}} m_{h,k} \times \\ \left[\begin{array}{l}\rho_{ads} R_m^2 \frac{2J_1(q_{h,k}R_m)}{q_{h,k}R_m}\exp\left[-\frac{(\sigma q_{h,k})^2}{2}\right] \\ -\rho_{ads} 2\pi^2 R_v^2 R_m^2 \times \\ \int_0^{2\pi} d\delta' \int_0^{\infty} dq_r'\, q_r' \frac{2J_1(q_r' R_m)}{q_r' R_m}\exp\left[-\frac{(\sigma q_r')^2}{2}\right] \frac{2J_1(\sqrt{q_{h,k}^2 + q_r'^2 - 2q_{h,k}q_r'\cos(\delta-\delta')}R_v)}{\sqrt{q_{h,k}^2 + q_r'^2 - 2q_{h,k}q_r'\cos(\delta-\delta')}R_v} \\ -\rho_{MCM-41} R_m^2 \frac{2J_1(q_{h,k}R_m)}{q_{h,k}R_m}\exp\left[-\frac{(\sigma q_{h,k})^2}{2}\right]\end{array}\right]^2\end{array}\right\} \quad (1)$$

where R_v as the radius of CD_4 vapor core and R_m as the nominal radius of matrix pore. ρ_v, ρ_{ads}, and ρ_{MCM-41} are neutron scattering length densities (SLDs) of the CD_4 vapor core, shell of adsorbed CD_4, and MCM-41 matrix, respectively. ρ_{MCM-41} is determined by a separate contrast variation SANS experiment to be $(3.66 \pm 0.009) \times 10^{10}$ cm^{-2}. σ is the diffusive parameter used to characterize the surface roughness of the MCM-41 pore wall. ρ_{ads} can be transferred to mass density of adsorbed CD_4 through the formula $\rho_{SLD} = \frac{\rho_{mass}}{M_w} N_A b$. $m_{h,k}$ is the multiplicity. *C* is a constant pre-factor related only to the length and number density of the cylindrical mesopores, and is independent of temperature if the amount of MCM-41 inside the neutron beam is the same during scattering measurements.

Equation (1) is a general formula for both empty MCM-41 matrix and CD_4/MCM-41 (both partially filled or fully filled mesopores). For empty MCM-41, R_v and ρ_{ads} are fixed as zero. For fully filled mesopores in MCM-41, R_v is fixed as zero and ρ_{ads} is a fitting parameter as confined fluid SLD.

7.2 Data Analysis

High q Background

To fit SANS data using equation (1), a linear background is added to the first order peak region and the *q* range below it. When plotting the intensity in *log-log* scale, the 2nd, 3rd and 4th peaks are grown on top of a linear line and this clearly suggests a power law background of this *q* range (see Figure 3). These backgrounds are used to account for the diffuse scattering of imperfect lattice

order of hexagonally packed structure and effects from other defects. Different backgrounds are used because the baseline of scattering pattern changes with q and temperature.

Porod Scattering

Porod scattering $I_p(q) = c_p \times q^{-4}$ is added to account for the low q upturn and Porod constant c_p is also a fitting parameter for each dataset. This low-q scattering is due to the contrast between the SLD of inter-particle space (vacuum or CD_4 vapor) and the average SLD of granular powder particles in the sample.

Resolution Function

To fit the experimental SANS data using the equation (1), the instrument resolution should be taken into account. The measured SANS intensity $I_M(q)$ can be expressed as

$$I_M(q) = \int \frac{I(q')}{\sqrt{2\pi\,\delta(q)^2}} \exp\left[-\frac{(q-q_m)^2}{2\,\delta(q)^2}\right] dq' \text{ , where } I(q') \text{ is the theoretical intensity calculated}$$

through equation (1) with q' as a dummy variable. The instrument resolution is approximated to be a Gaussian function with the standard deviation $\delta(q)$ and q dependent parameter q_m.

Fitting Procedures

(i) Empty MCM-41 matrix is measure first in order to determine matrix structural information. For empty MCM-41, R_v and ρ_{ads} are fixed as zero and equation (1) reduces to

$$\lim_{q_{h,k}L\to\infty} I(q_{h,k}) = C\sum_{h,k}\left\{\frac{1}{q_{h,k}}\, m_{h,k}\left[\rho_{MCM-41}R_m^2\,\frac{2J_1(q_{h,k}R_m)}{q_{h,k}R_m}\exp\left[-\frac{(\sigma\, q_{h,k})^2}{2}\right]\right]^2\right\}$$

$\rho_{MCM\text{-}41}$ is fixed as $(3.66 \pm 0.009) \times 10^{10}$ cm^{-2} and the fitting parameters are C, σ, R_m, and Porod constant c_p.

(ii) Once C, σ, and R_m are known, they are fixed as known parameter for the gas loading cases. By using equation (1), the only fitting parameters are R_v, ρ_{ads}, and c_p together with the background functions.

(iii) After vapor-liquid transition, the mesopores are fully filled with CD_4 liquid or solid and therefore R_v is fixed as zero. The only fitting parameter are ρ_{ads} and c_p. Here ρ_{ads} is the confined methane density. It should be noted that even though using R_v as a fitting parameter, the obtained value should be a number very close to zero.

Absolute Adsorption Amount

Absolute adsorption per length, M_{ads}, is calculated from integrating the mass density of CD_4 over a mesopore with diffuse surface. It is expressed as $M_{ads} = \int_0^\infty \rho_{CD_4,mass}\,\varphi_{GA}(r)\,2\pi r\,dr$. M_{ads} is a

function of R_v and $\rho_{CD_4,mass}$. $\varphi_{GA}(r)$ is the gas accessible volume fraction and it decreases to 0 when r approaches to the dense silica matrix region.

8. Questions to answer:

SANS is a powerful tool to study gas adsorption mechanism in the mesoporous materials. After data analysis, you should be able to get the vapor core radius R_v, the scattering length density and mass density of adsorbed CD_4, and absolute adsorption per length as a function of temperature.

Reference

(1) Shale gas provides largest share of U.S. natural gas production in 2013 - Today in Energy - U.S. Energy Information Administration (EIA) http://www.eia.gov/todayinenergy/detail.cfm?id=18951 (accessed Jul 7, 2015).

(2) • U.S. energy - shale gas production 2014 | Statistic http://www.statista.com/statistics/183740/shale-gas-production-in-the-united-states-since-1999/ (accessed Oct 6, 2014).

(3) Loucks, R. G.; Reed, R. M.; Ruppel, S. C.; Jarvie, D. M. Morphology, Genesis, and Distribution of Nanometer-Scale Pores in Siliceous Mudstones of the Mississippian Barnett Shale. *J. Sediment. Res.* **2009**, *79* (12), 848–861.

(4) Ambrose, R. J.; Hartman, R. C.; Diaz Campos, M.; Akkutlu, I. Y.; Sondergeld, C. New Pore-Scale Considerations for Shale Gas in Place Calculations. In *SPE Unconventional Gas Conference*; Society of Petroleum Engineers, 2013.

(5) Corma, A. From Microporous to Mesoporous Molecular Sieve Materials and Their Use in Catalysis. *Chem. Rev.* **1997**, *97* (6), 2373–2420.

(6) Chang, F.; Zhou, J.; Chen, P.; Chen, Y.; Jia, H.; Saad, S. M. I.; Gao, Y.; Cao, X.; Zheng, T. Microporous and Mesoporous Materials for Gas Storage and Separation: A Review. *Asia-Pacific J. Chem. Eng.* **2013**, *8* (4), 618–626.

(7) Vartuli, J. C.; Schmitt, K. D.; Kresge, C. T.; Roth, W. J.; Leonowicz, M. E.; McCullen, S. B.; Hellring, S. D.; Beck, J. S.; Schlenker, J. L. Effect of Surfactant/Silica Molar Ratios on the Formation of Mesoporous Molecular Sieves: Inorganic Mimicry of Surfactant Liquid-Crystal Phases and Mechanistic Implications. *Chem. Mater.* **1994**, *6* (12), 2317–2326.

(8) Beck, J. S.; Vartuli, J. C.; Roth, W. J.; Leonowicz, M. E.; Kresge, C. T.; Schmitt, K. D.; Chu, C. T. W.; Olson, D. H.; Sheppard, E. W. A New Family of Mesoporous Molecular Sieves Prepared with Liquid Crystal Templates. *J. Am. Chem. Soc.* **1992**, *114* (27), 10834–10843.

(9) Kresge, C. T.; Leonowicz, M. E.; Roth, W. J.; Vartuli, J. C.; Beck, J. S. Ordered Mesoporous Molecular Sieves Synthesized by a Liquid-Crystal Template Mechanism. *Nature* **1992**, *359* (6397), 710–712.

(10) Sayari, A.; Yang, Y.; Kruk, M.; Jaroniec, M. Expanding the Pore Size of MCM-41 Silicas: Use of Amines as Expanders in Direct Synthesis and Postsynthesis Procedures. *J. Phys. Chem. B* **1999**, *103* (18), 3651–3658.

(11) Muroyama, N.; Yoshimura, A.; Kubota, Y.; Miyasaka, K.; Ohsuna, T.; Ryoo, R.; Ravikovitch, P. I.; Neimark, A. V.; Takata, M.; Terasaki, O. Argon Adsorption on MCM-41 Mesoporous Crystal Studied by In Situ Synchrotron Powder X-Ray Diffraction. *J. Phys. Chem. C* **2008**, *112* (29), 10803–10813.

(12) Tanaka, H.; Hiratsuka, T.; Nishiyama, N.; Mori, K.; Miyahara, M. T. Capillary Condensation in Mesoporous Silica with Surface Roughness. *Adsorption* **2013**, *19* (2-4), 631–641.
(13) Chiang, W.-S.; Fratini, E.; Baglioni, P.; Georgi, D.; Chen, J.; Liu, Y. Methane Adsorption in Model Mesoporous Material, SBA-15, Studied by Small-Angle Neutron Scattering. *J. Phys. Chem. C* **2016**, *120* (8), 4354–4363.
(14) Liu, D.; Zhang, Y.; Chen, C.-C.; Mou, C.-Y.; Poole, P. H.; Chen, S.-H. Observation of the Density Minimum in Deeply Supercooled Confined Water. *Proc. Natl. Acad. Sci.* **2007**, *104* (23), 9570–9574.
(15) King, H. E.; Eberle, A. P. R.; Walters, C. C.; Kliewer, C. E.; Ertas, D.; Huynh, C. Pore Architecture and Connectivity in Gas Shale. *Energy & Fuels* **2015**, *29* (3), 1375–1390.
(16) Ritter, H.; Nieminen, M.; Karppinen, M.; Brühwiler, D. A Comparative Study of the Functionalization of Mesoporous Silica MCM-41 by Deposition of 3-Aminopropyltrimethoxysilane from Toluene and from the Vapor Phase. *Microporous Mesoporous Mater.* **2009**, *121* (1-3), 79–83.
(17) This Section Is a Revised Version Based on the Course Material in 2010 NCNR Neutron Summer School. (https://www.ncnr.nist.gov/summerschool/ss10/pdf/Handout_NG3SANS_FlowSANS.pdf)